

1 **Supplementary material to “Influence of Surface Morphology on the Immersion Mode Ice**
2 **Nucleation Efficiency of Hematite Particles”**

3
4 **December 17, 2013**

5
6 Naruki Hiranuma^{a,*}, Nadine Hoffmann^a, Alexei Kiselev^a, Axel Dreyer^{b,†}, Kai Zhang^c,
7 Gourihar Kulkarni^c, Thomas Koop^b, and Ottmar Möhler^a

8
9
10 ^a*Institute for Meteorology and Climate Research – Atmospheric Aerosol Research, Karlsruhe*
11 *Institute of Technology, Karlsruhe, Germany.*

12 ^b*Faculty of Chemistry, Bielefeld University, Bielefeld, Germany.*

13 [†]*Now at Institute Advanced Ceramics, Hamburg University of Technology, Hamburg, Germany*

14 ^c*Atmospheric Science and Global Change Division, Pacific Northwest National Laboratory,*
15 *Richland, Washington, USA*

16
17
18 *Corresponding Author. E-mail: seong.moon@kit.edu

19

20

21

22

23

24

25

26 **Citation:**

27 N. Hiranuma, N. Hoffmann, A. Kiselev, A. Dreyer, K. Zhang, G. Kulkarni, T. Koop, and O.
28 Möhler. **Influence of Surface Morphology on the Immersion Mode Ice Nucleation Efficiency**
29 **of Hematite Particles**, for *Atmospheric Chemistry and Physics*

30 This supplementary information provides additional details in the measurement of
31 absolute number of charges by polyelectrolyte titrations with PVS and PDADMAC (Table S1) as
32 well as representative AIDA adiabatic expansion experiments (Figure S1 and S2).

33 Below, we briefly describe an experimental procedure to estimate maximal charge
34 densities of hematite particles. First, we generated the maximal interface potentials in hematite
35 suspensions by adding 0.01 mol L⁻¹ NaOH or HCl solution. Compensations of the developed
36 charges in the suspensions were directly followed and carried out by adding the oppositely
37 charged polyelectrolyte solution (PVS or PDADMAC) to zero potential to identify the absolute
38 number of surface charges. With measured and known parameters summarized in Table S1, we
39 calculated the maximal charge surface densities, a (nm⁻²), according to

$$41 \quad a = \frac{c_{eq} \cdot V \cdot N_A}{m \cdot A_{BET}} \quad (S1)$$

42
43 where c_{eq} is the polyelectrolyte charge equivalent concentration (mol L⁻¹), V is the titrated
44 volume to isoelectric point (L), N_A is the Avogadro's constant (mol⁻¹), m is the hematite mass (g)
45 and A_{BET} is the BET specific surface area (m² g⁻¹). We note that 1 mol L⁻¹ of polyelectrolyte
46 concentration compensates 400 charges.

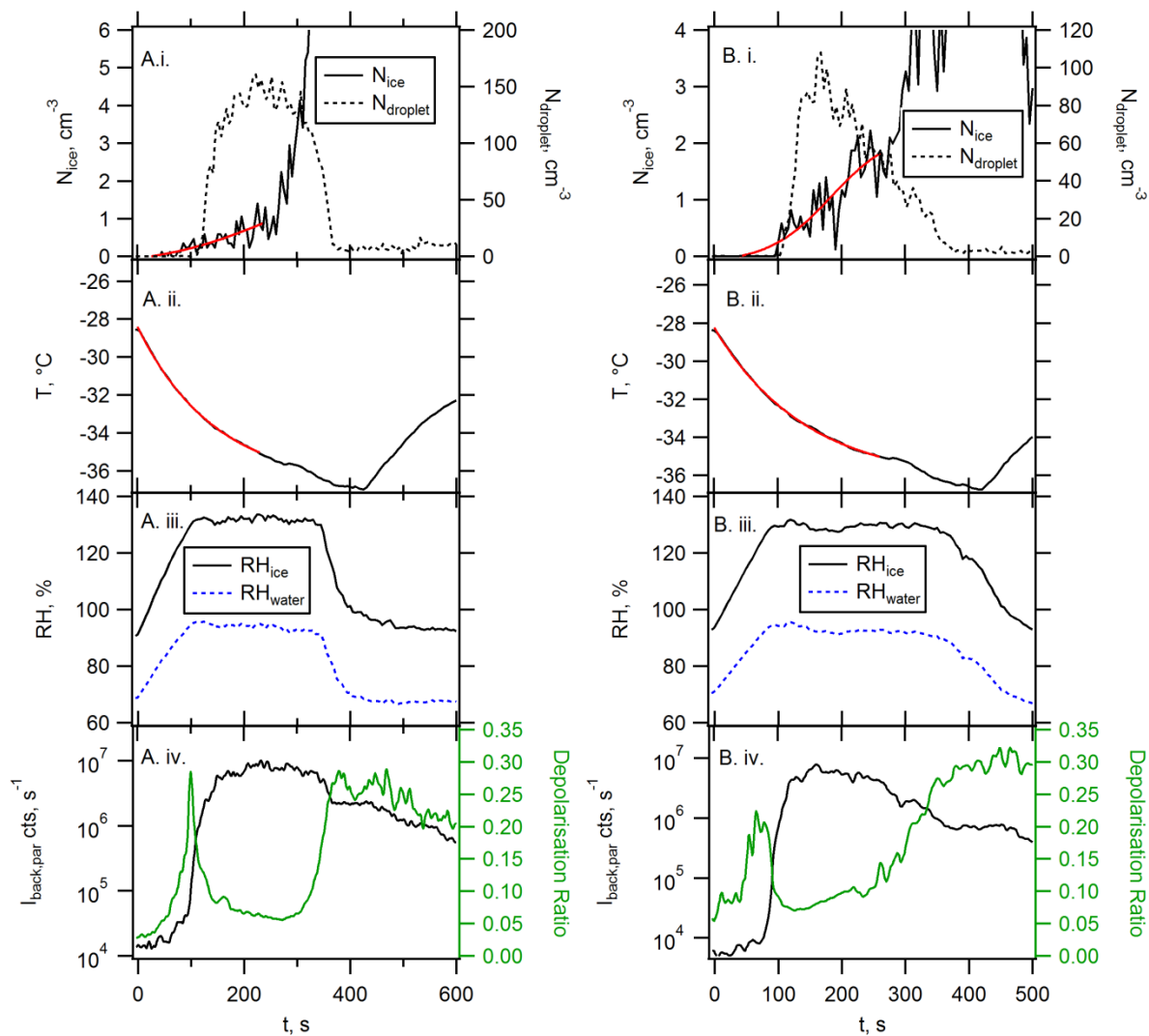
47 Figure S1 displays the time-series of ice crystal concentration (N_{ice}) as well as liquid
48 droplet concentration ($N_{droplet}$), temperature (T), relative humidity with respect to ice and water
49 measured by the TDL, and particle phase inferred by particles' backscattered intensities to the
50 incident polarisation state of the laser light during the immersion mode freezing experiment for
51 cubic hematite and milled hematite particles shown in Manuscript Figure 2 (INUIT04_13 and
52 INUIT04_15, respectively). It is noteworthy that the observed early increases in depolarisation
53 ratio before the full droplet formation at water saturation are the indicator of deposition mode
54 freezing (Figure S1 A. iv. and B. iv.). As prescribed in Manuscript Section 3.2, the contributions
55 of depositional ice formation to the total ice crystals formed through an expansion (up to 27%)
56 was too small to inhibit new ice formation in the immersion mode after reaching to the water
57 supersaturation condition (i.e. no indication of water depletion until homogeneous freezing
58 emerges). Therefore, the ice crystals formed through deposition mode freezing were simply

59 subtracted from the total number of ice crystals measured within heterogeneous freezing regime
60 to compute n_s solely accounting for the immersion mode ice nucleation.

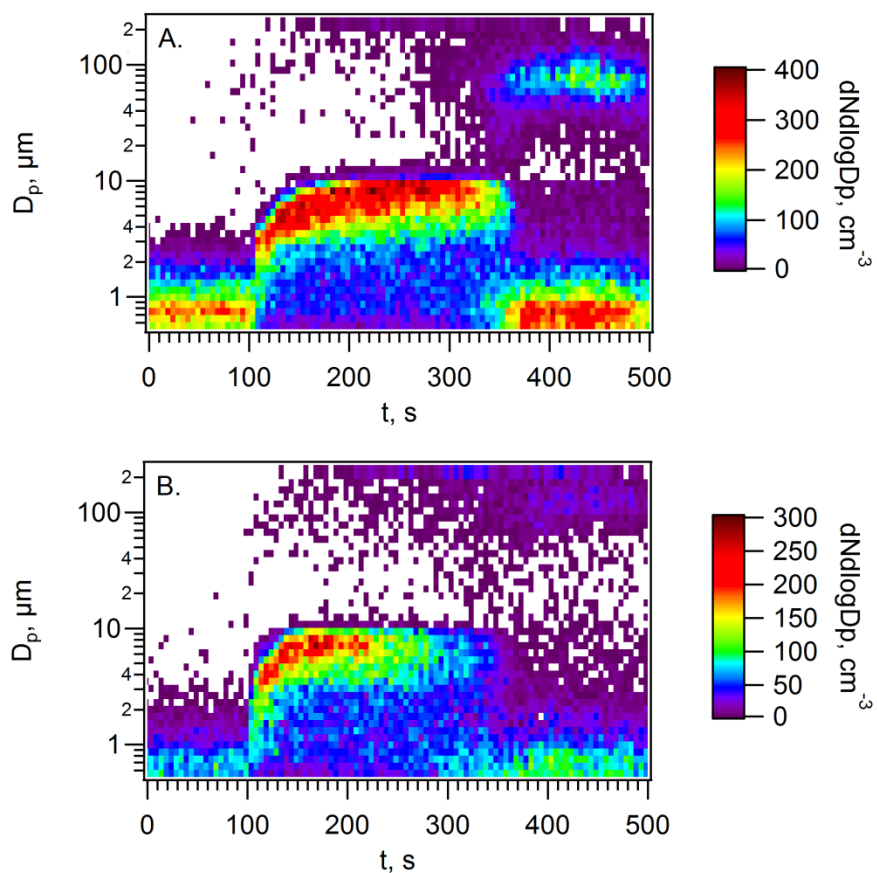
61 Figure S2 illustrates the size distributions of particles, droplets, and ice crystals measured
62 by the WELAS. Observed size growth initiated around 100 s was triggered by droplet formation.
63 Particles above 20 μm diameter were counted as ice crystals. The contributions from
64 homogeneous ice nucleation appear below $-35\text{ }^\circ\text{C}$. Soon after that point, abrupt increase in
65 depolarisation ratio and quick decrease in water saturation were observed, which implies the
66 presence of pure ice cloud (Figure S1).

67 Table S1. Summary of parameters used to calculate the charge densities, a (nm^{-2}), of cubic and
 68 milled hematite particles. PVS and PDADMAC solutions were used to obtain maximal positive
 69 and maximal negative charge densities, respectively.
 70

Hematite	c_{eq} , 10^{-5} mol L $^{-1}$	V , 10^{-3} L	m , 10^{-3} g	A_{BET} , $\text{m}^2 \text{g}^{-1}$	a , nm^{-2}
Cubic (max. positive)	1 \pm 0.009	1.91 \pm 0.01	10.1 \pm 0.1	2.2 \pm 0.1	0.36 \pm 0.03
Cubic (max. negative)	10 \pm 0.090	1.15 \pm 0.01	10.1 \pm 0.1	2.2 \pm 0.1	1.39 \pm 0.03
Milled (max. positive)	1 \pm 0.009	1.83 \pm 0.01	8.2 \pm 0.1	3.7 \pm 0.1	0.52 \pm 0.05
Milled (max. negative)	1 \pm 0.009	7.02 \pm 0.01	8.2 \pm 0.1	3.7 \pm 0.1	3.13 \pm 0.05



72
 73 Figure S1. Typical experimental profiles, including i. ice crystal concentration (N_{ice}) and liquid
 74 droplet concentration ($N_{droplet}$), ii. temperature (T), iii. TDL, and iv. SIMONE measurements, of
 75 the AIDA immersion mode ice nucleation experiment for A. cubic hematite particles
 76 (INUIT04_13) and B. milled hematite particles (INUIT04_15). Note that the red lines represent
 77 interpolated data. The $I_{back,par}$ in Panel A.iv and B.iv denotes backscattered light scattering
 78 intensity parallel to the incident polarisation state (log-scaled).



80
81 Figure S2. Time-series of the WELAS size distribution of the AIDA immersion mode ice
82 nucleation experiment for A. cubic hematite particles (INUIT04_13) and B. milled hematite
83 particles (INUIT04_15).